

Headline Articles

UV and Visible Emission Spectra from the Photodissociation of Carbonyl Sulfide Using Synchrotron Radiation at 15–30 eV

Koichiro Mitsuke* and Masakazu Mizutani

Department of Vacuum UV Photo-Science, Institute for Molecular Science and Department of Structural Molecular Science, The Graduate University for Advanced Studies, Myodaiji, Okazaki 444-8585

(Received January 22, 2001)

The photofragmentation of OCS at photon energies of 15–30 eV has been studied by dispersed fluorescence spectroscopy. The primary photon beam was monochromatized undulator radiation supplied from the UVSOR facility. The following emission-band systems have been identified: $\text{OCS}^+[\text{A}^2\Pi_{g^2}(0,0,0) \rightarrow \text{X}^2\Pi_{g^2}(0,0,v_3'')]$, $\text{CO}^+(\text{A}^2\Pi_{g^2} \rightarrow \text{X}^2\Sigma^+)$, $\text{CS}^+(\text{B}^2\Sigma^+ \rightarrow \text{A}^2\Pi_{g^2})$, and $\text{CO}(d^3\Delta \rightarrow a^3\Pi)$. All of the transitions, except for $\text{OCS}^+[\text{A}^2\Pi_{g^2} \rightarrow \text{X}^2\Pi_{g^2}]$, were first observed in the vacuum UV photodissociation of OCS. The fluorescence excitation spectra for the $\text{OCS}^+[\text{A}^2\Pi_{g^2}(0,0,0) \rightarrow \text{X}^2\Pi_{g^2}(0,0,v_3'')]$ and $\text{CS}^+(\text{B}^2\Sigma^+ \rightarrow \text{A}^2\Pi_{g^2})$ transitions were measured in the photon energy range of 15.1–15.75 and 21.8–26 eV, respectively. The emission spectra obtained at 20.85 and 22.9 eV exhibit atomic transitions of $\text{S}[nd^3\text{D}^o \rightarrow 4p^3\text{P}^e (n = 6-9)]$, which result from the neutral dissociation of superexcited Rydberg states of OCS into $\text{S}(nd^3\text{D}^o) + \text{CO}$. Possible excited states of the counterpart CO are discussed on the basis of the difference in the n distribution between the two spectra.

When molecules are electronically excited by absorbing vacuum ultraviolet (VUV) photons, they usually decay into many sorts of ionic and neutral photofragmentation products.¹⁻⁵ In some cases, the fragments possess sufficient internal energy to de-excite radiatively by emitting UV or visible fluorescence. In the early 1970's, Lee and Judge accomplished pioneering work on the fluorescence spectroscopy of various molecules photoexcited in the VUV region.^{6,7} Later, Nenner and coworkers^{1,8} as well as Ukai, Hatano and coworkers⁹⁻¹² studied the direct dissociation and predissociation of ionic or superexcited states produced by VUV excitation using synchrotron radiation by means of fluorescence excitation spectroscopy and two-dimensional fluorescence spectroscopy. It is widely accepted that fluorescence spectroscopy is an important tool to determine the fragments and to clarify the mechanisms governing the dissociation processes of diatomic and polyatomic molecules.

Lee and Judge measured the dispersed fluorescence spectra of carbonyl sulfide, OCS, by utilizing seven discrete emission lines between $E_{\text{hv}} = 15.48$ – 19.46 eV and assigned the dominant features to the $\text{OCS}^+[\text{A}^2\Pi_{g^2}(0,0,0) \rightarrow \text{X}^2\Pi_{g^2}(v_1,0,v_3)]$ transitions.¹³ Here, E_{hv} denotes the excitation photon energy. Tabché-Fouhaile et al. reported on the fluorescence excitation spectra of OCS in the region of $E_{\text{hv}} = 11.1$ – 18.5 eV.¹⁴ The observed fluorescence emissions with wavelengths of 160–300 nm and 530–630 nm were ascribed chiefly to $\text{CS}(\text{A}^1\Pi)$ and

$\text{CO}(a'^3\Sigma^+, d^3\Delta, e^3\Sigma^-)$, respectively, produced by predissociation of the Rydberg series converging to $\text{OCS}^+(\text{B}^2\Sigma^+)$. However, the emitting fragments were not definitely identified in their work, since they employed only optical filters to confine the wavelength region of the fluorescence. The energy-level diagram in Fig. 1 summarizes the dissociation limits of OCS for the formation of neutral and cation fragments. An increase in E_{hv} is expected to drastically promote the formation of radiative fragments. Nevertheless, at $E_{\text{hv}} > 15$ eV, the fluorescing transitions which were dispersed and detected by a monochromator were limited only to $\text{OCS}^+(\text{A}^2\Pi_{g^2} \rightarrow \text{X}^2\Pi_{g^2})$ and $\text{CS}(\text{A}^1\Pi \rightarrow \text{X}^1\Sigma^+)$.^{13,15} Moreover, there has been no experimental work on the fluorescence spectroscopy of any neutral or cation fragments from OCS at $E_{\text{hv}} > 20$ eV. As suggested from Fig. 1, the VUV photon in this region has sufficient energy to cause a prompt dissociation of OCS into a fragment ion emitting a UV or visible photon.

The present paper describes the fluorescence (emission) spectra of OCS measured in the region $E_{\text{hv}} = 15$ – 30 eV. In order to improve the detection efficiency, we developed an optical detection system consisting of spheroidal and spherical mirrors in combination with an optical-fiber bundle. The detection limit for the partial fluorescence cross section is estimated to be less than 10^{-3} Mb. This improvement allows us to perceive weak fluorescence signals of fragments from OCS photoexcited in the VUV region.

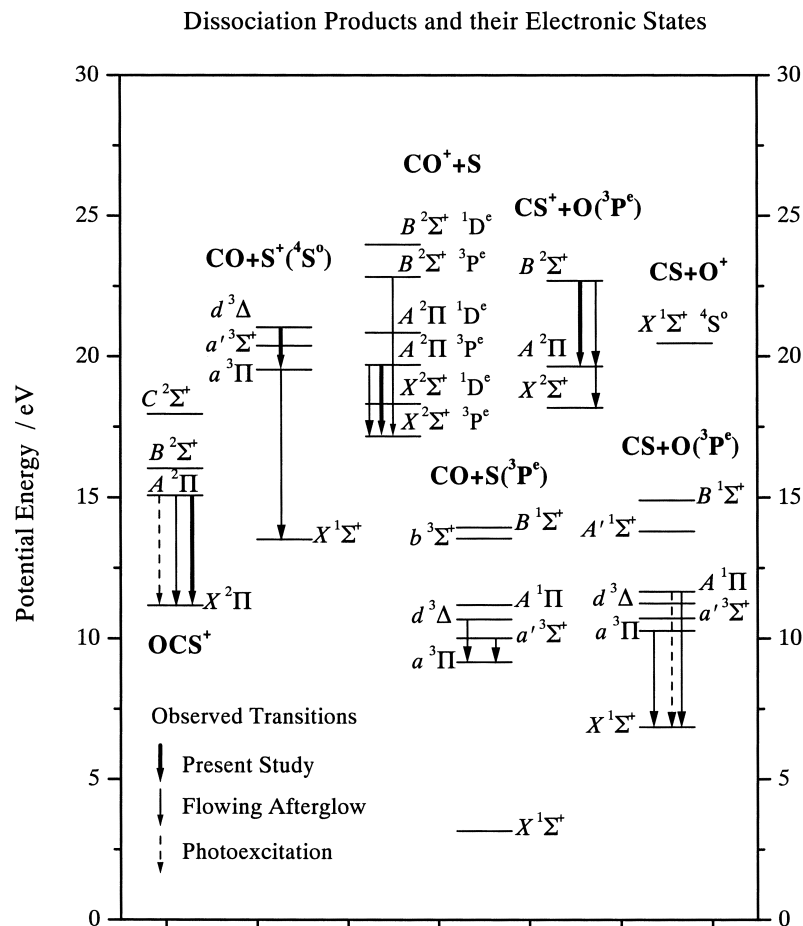


Fig. 1. Energy level diagram illustrating the adiabatic ionization potentials (Ref. 42) and dissociation limits of OCS. Data taken from Refs. 19, 21, 28, 37, and 38 are used to calculate the dissociation limits (see also Table 1 of Ref. 43). All energies are measured with respect to the neutral ground state of $\text{OCS}[X^1\Sigma^+(0,0,0)]$. Thick, thin, and dashed arrows indicate the transitions identified in the synchrotron radiation photoexcitation (present study), in flowing rare gas afterglow reactions (Refs. 23–27 and 44), and in the photoexcitation at the photon energy above 15 eV (Refs. 13 and 15), respectively.

Experimental

All experiments were carried out at beam line 3A2 of the UV-SOR facility in the Institute for Molecular Science. Details of the undulator radiation are described elsewhere.^{5,16} Carbonyl sulfide OCS was expanded under an effusive jet condition through a multichannel capillary plate, and subjected to the irradiation of monochromatized undulator radiation ($E_{\text{hv}} = 15\text{--}29.8$ eV). Commercial high-purity gas (Matheson, 97.5% pure) was used without any further purification. The fundamental light of the undulator radiation was dispersed by a monochromator of constant deviation grazing-incidence type with a 2.2 m focal length. The monochromator can cover a wide wavelength range of $\sim 10\text{--}95$ nm by interchanging three spherical gratings: G1 (600 grooves mm^{-1}) at 95.3–22.5 nm, G2 (1200 grooves mm^{-1}) at 53.8–12.4 nm, and G3 (2400 grooves mm^{-1}) at 27–9.9 nm. However, G1 was used in almost all experimental runs. The size of the monochromatized light was ca. 1×1 mm^2 at the intersection region. A typical photon intensity and spectral resolution of the synchrotron radiation were 7.8×10^{14} photons $\text{s}^{-1} \text{cm}^{-2}$ and 2.4 Å (FWHM, 83 meV at 20.85 eV), respectively, with entrance- and exit-slit widths of 300 μm . There exists contamination of the light by passage of a second order through the monochromator from the second undulator

harmonic. The concentration of the second-order light was estimated to be no less than 10% at $E_{\text{hv}} = 15$ eV.

The fluorescence was collected by an optical detection system, as shown in Fig. 2. Spheroidal and spherical mirrors were mounted so that their surfaces would face each other across the photoexcitation region (*PR*), i.e. the source of the fluorescence. One focal point of the spheroidal mirror fell at *PR*, while the other focal point was at the surface of an optical-fiber bundle of 50 cm long. The fluorescence light was reflected back to *PR* by the spherical mirror with its focal point at *PR*, and was then focused onto the surface of the fiber bundle by the spheroidal mirror. This detection system could collect light from about 62% of the full-sphere solid angle. The fluorescence passed through the optical-fiber bundle, whose transmission was estimated to be 55% at 400 nm.

Two types of monochromators were used to disperse the fluorescence. In dispersed fluorescence spectroscopy we utilized a 300 mm focal-length imaging spectrograph (Roper Scientific, SpectraPro-300i, Tzerny–Taner type) equipped with a liquid-nitrogen cooled CCD array detector of 26.8 mm wide (the dispersion direction) and 2 mm high. Unless otherwise mentioned, a 600 grooves mm^{-1} grating having a nominal blaze wavelength of 500 nm was used. The overall detection efficiency, including the spheroidal and spherical mirrors, fiber bundle, and imaging spec-

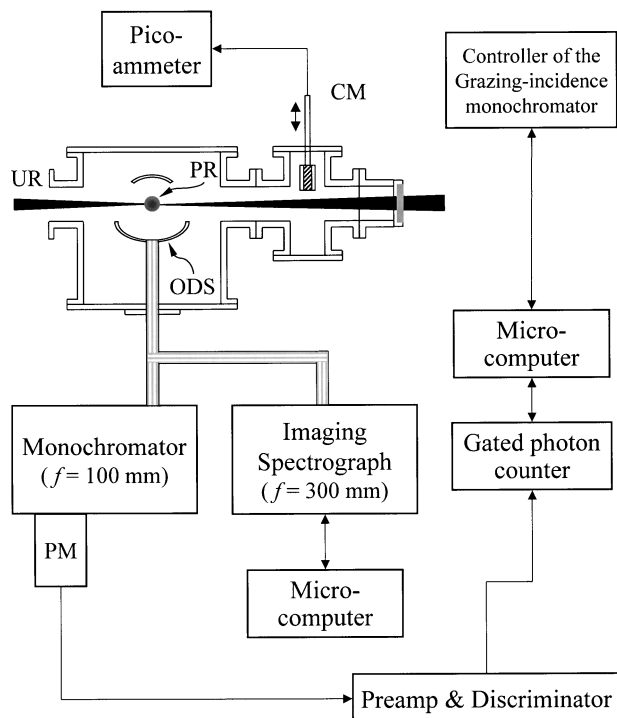


Fig. 2. Schematic diagram of the apparatus for dispersed fluorescence spectroscopy and fluorescence excitation spectroscopy. UR, monochromatized undulator radiation; PR photoexcitation region (not to scale); ODS, optical detection system composed of spheroidal and spherical mirrors and an optical-fiber bundle; CM, gold-mesh current monitor; PM, photomultiplier.

trograph, was estimated to be $(1.1 \pm 0.3) \times 10^{-3}$ with the entrance slit width of the spectrograph being 250 μm . When we fulfilled fluorescence excitation spectroscopy by scanning the wavelength of synchrotron radiation, we replaced the imaging spectrograph by a 100 mm focal-length monochromator (Ritu, MC10N, 600 grooves mm^{-1} grating) and a photomultiplier tube (Hamamatsu, R464S). In this case, the overall detection efficiency, including the mirrors, fiber bundle, monochromator, and photomultiplier tube, was estimated to be $(1.4 \pm 0.3) \times 10^{-3}$ at the entrance- and exit-slit widths of the monochromator of 2 mm. All spectra given in the present paper were corrected by the wavelength dependence of the relative detection efficiency.

Results and Discussion

Observed Emission at Fluorescence Wavelengths of 360–530 nm. Figure 3 shows dispersed fluorescence spectra at the wavelength region 360–530 nm measured at five E_{hv} points between 19.85 and 29.8 eV. The electronic transitions of two kinds of ions are clearly observed: $\text{OCS}^+[\text{A}^2\Pi_{\Omega}(0,0,0) \rightarrow \text{X}^2\Pi_{\Omega}(0,0,v_3'')]$ with $v_3'' = 2\text{--}5$ and $\text{CO}^+(\text{A}^2\Pi_{\Omega}, v' \rightarrow \text{X}^2\Sigma^+, v'')$. Quenching of the excited ions in collisions with ambient molecules can be disregarded, because the sample pressure at the intersection region was of the order of 10^{-3} Pa, and because the fluorescence lifetime of $\text{OCS}^+[\text{A}^2\Pi_{\Omega}(0,0,0)]$ and $\text{CO}^+(\text{A}^2\Pi_{\Omega}, v')$ are ~ 0.17 and $2.1\text{--}3.0$ μs , respectively.^{17,18} Obviously, the observed transitions result from unimolecular decay processes. The vibrational progression of the $\text{OCS}^+[\text{A}^2\Pi_{\Omega}(0,0,0) \rightarrow \text{X}^2\Pi_{\Omega}(0,0,v_3'')]$ transition shows promi-

nent spin-orbit doublet structures, specified by $\Omega = 3/2$ and $1/2$. A photoionization study at $E_{\text{hv}} < 20$ eV indicates that the emission of $\text{OCS}^+[\text{A}^2\Pi_{\Omega}(0,0,0)]$ gives the most intense bands in the UV and visible regions upon photoexcitation in OCS.¹³ The $\text{CO}^+(\text{A}^2\Pi_{\Omega}, v' \rightarrow \text{X}^2\Sigma^+, v'')$ emission-band system up to $v' = 4$ clearly appears at $E_{\text{hv}} \geq 20.85 \pm 0.04$ eV. On the other hand, no vibrational band of $\text{CO}^+(\text{A}^2\Pi_{\Omega}, v')$ was identified when E_{hv} was lowered to 19.85 ± 0.04 eV. At this energy, only the $v' = 0$ state of $\text{CO}^+(\text{A}^2\Pi_{\Omega})$ can be produced, since the thermochemical thresholds^{19–21} for the formation of $\text{S}(\text{P}^{\text{p}}) + \text{CO}^+(\text{A}^2\Pi_{\Omega}, v')$ with $v' = 0$ and 1 lie at 19.70 ± 0.015 and 19.89 ± 0.015 eV, respectively. The $v' = 0 \rightarrow v'' = 0$ transition at 490 nm is relatively weak because of an unfavorable Franck–Condon overlap,²² and may be almost smeared out at $E_{\text{hv}} = 19.85$ eV. Several authors have studied the $\text{CO}^+(\text{A}^2\Pi_{\Omega}, v' \rightarrow \text{X}^2\Sigma^+, v'')$ emission-band system resulting from Penning ionization or excitation transfer of OCS in collisions with rare gas metastable atoms or ions, respectively.^{23–28} In contrast, no investigation has been made on the production of $\text{CO}^+(\text{A}^2\Pi_{\Omega}, v')$ as an emitting species from photo-irradiated OCS molecules.

With increasing E_{hv} , the intensity ratio of the $\text{CO}^+(\text{A}^2\Pi_{\Omega}, v' \rightarrow \text{X}^2\Sigma^+, v'')$ bands to that of $\text{OCS}^+[\text{A}^2\Pi_{\Omega}(0,0,0) \rightarrow \text{X}^2\Pi_{\Omega}(0,0,v_3'')]$ gradually increases. Another distinct trend of the spectra is an enhancement of the broad feature encompassing the 405–420 nm region. Somewhere between $E_{\text{hv}} = 22.9$ and 25.0 eV a reversal seems to occur in the intensities of this feature at 405–420 nm and the $\text{CO}^+(\text{A}^2\Pi_{\Omega}, v' = 3 \rightarrow \text{X}^2\Sigma^+, v'' = 0)$ band around 400–405 nm. The fluorescence intensity in the wavelength region of 400–410 nm was measured as a function of E_{hv} using the 100 mm focal-length monochromator. The resultant fluorescence excitation spectrum of OCS is depicted in Fig. 4. The fluorescence intensity shows a slow onset at 23 ± 0.5 eV. This observation leads us to infer that the new feature at 405–420 nm in Fig. 3 can be attributed to the bands originating from the $\text{CS}^+(\text{B}^2\Sigma^+ \rightarrow \text{A}^2\Pi_{\Omega})$ transition, since the thermochemical threshold^{19,29,30} for the formation of $\text{CS}^+(\text{B}^2\Sigma^+)$ from OCS is 22.76 eV. A vibrational analysis of this band system was first carried out by Tsuji et al. in 1980.²⁴ In their experiment, $\text{CS}^+(\text{B}^2\Sigma^+)$ fragments were formed by thermal energy charge transfer from He^+ to OCS in flowing helium afterglow reactions. To compare the present data with their high-resolution spectrum²⁴ ($\Delta\lambda = 0.08$ nm) we acquired an expanded dispersed fluorescence spectrum (Fig. 5) taken at $E_{\text{hv}} = 25.05$ eV. Here, a 1200 grooves mm^{-1} grating with a nominal blaze wavelength of 300 nm was mounted in the 300 mm focal-length imaging spectrograph. Figure 5 includes the reported positions²⁴ of the $\Delta v = v' - v'' = 0$ sequences of the two spin-orbit components ($\Omega = 3/2$ and $1/2$) of the $\text{CS}^+(\text{B}^2\Sigma^+, v' \rightarrow \text{A}^2\Pi_{\Omega}, v'')$ transition. Weak maxima observed at ~ 406 and ~ 411 nm in the present spectrum, which were reproducible on triplicate experimental runs, appear to be consistent with the accepted band features in the $\text{CS}^+(\text{B}^2\Sigma^+ \rightarrow \text{A}^2\Pi_{\Omega})$ system.

Cross Section for the $\text{OCS}^+(\text{A} \rightarrow \text{X})$ Fluorescence. The fluorescence cross section σ_f of $\text{OCS}(\text{X}^1\Sigma^+)$ for the $\text{OCS}^+[\text{A}^2\Pi_{3/2}(0,0,0) \rightarrow \text{X}^2\Pi_{3/2}(0,0,3)]$ transition at 394.5 nm was evaluated to be 5×10^{-3} Mb at $E_{\text{hv}} = 20.85$ eV by calibrating its signal count rate against that of the $\text{N}_2^+(\text{B}^2\Sigma_u^+, v' =$

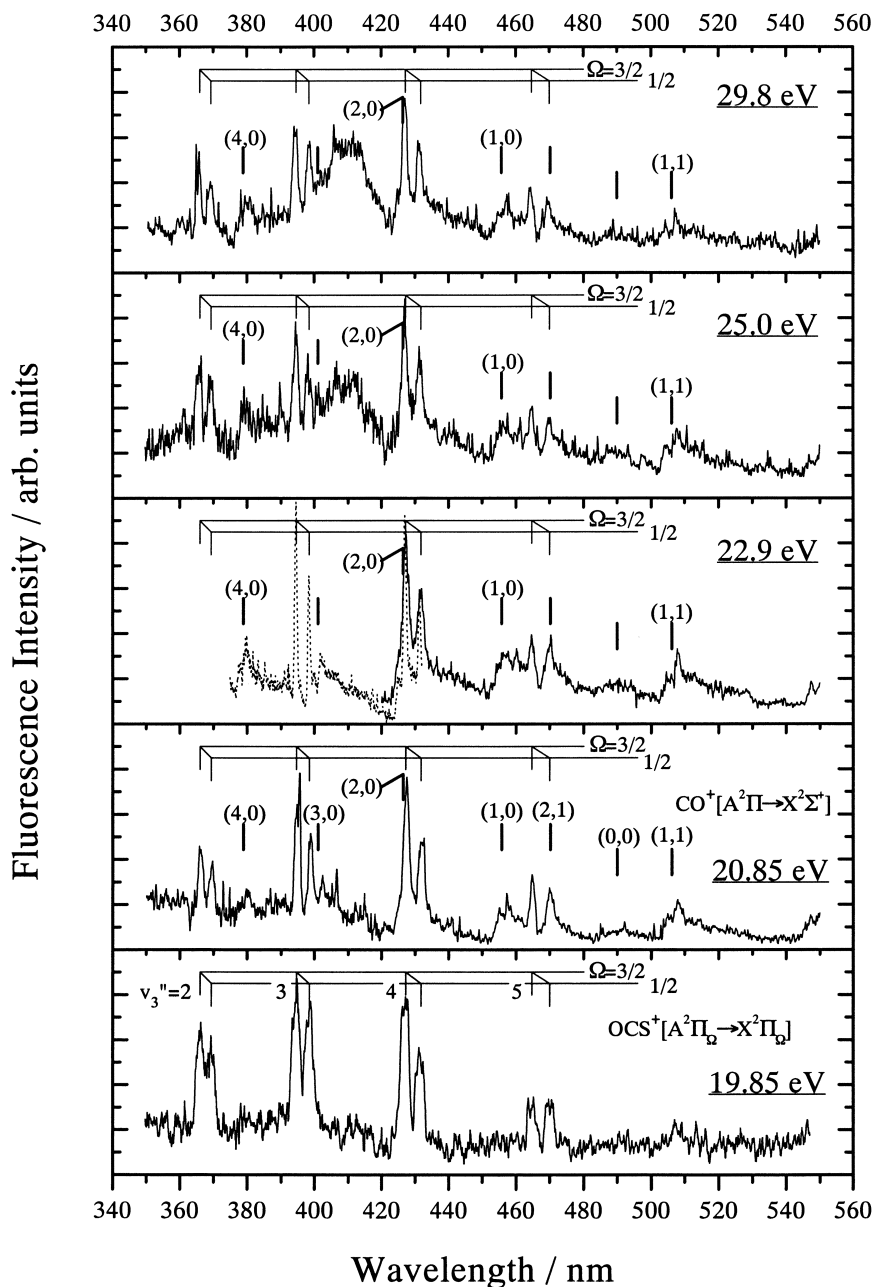


Fig. 3. Dispersed fluorescence spectra of OCS encompassing the wavelength region 360–530 nm at five photon energies between 19.85 and 29.8 eV. The imaging spectrograph equipped with a 600 grooves mm^{-1} grating (blaze wavelength = 500 nm) was used at the entrance-slit width of 500 μm at $E_{\text{hv}} = 19.85$ eV and 250 μm at the other four photon energies. A 1200 grooves mm^{-1} grating (blaze wavelength = 300 nm) was employed to obtain the dashed curve in the panel of $E_{\text{hv}} = 22.9$ eV. The thin vertical lines indicate the vibrational progression in the antisymmetric stretch v_3 mode of the OCS⁺[A²Π_g(0,0,0) → X²Π_g(0,0,v₃'')] transition. The number of the excited quanta are given in the panel of $E_{\text{hv}} = 19.85$ eV. The thick vertical lines indicate the band origins of the CO⁺(A²Π_g, v' → X²Σ⁺, v'') emission-band system. The (v', v'') mark denotes the band due to the transition from the upper v' to lower v'' vibrational states.

$0 \rightarrow X^2\Sigma_g^+$, v'' = 0) emission of N₂ at 389–392 nm. In the calibration procedure, a N₂ sample was admitted into the photoexcitation region, instead of OCS. We adopt the following equation to connect σ_f with the signal count rate S :

$$S = n\sigma_f i_{\text{eff}} \eta V. \quad (1)$$

Here, n is the number density of the sample, i_{eff} the effective photon intensity at the interaction region, η the overall collection efficiency of the detection system, and V the interaction volume. The fluorescence cross section of N₂ for the N₂⁺(B²Σ_u⁺, v' = 0 → X²Σ_g⁺, v'' = 0) transition is assumed to be equal to the product of the partial photoionization cross sec-

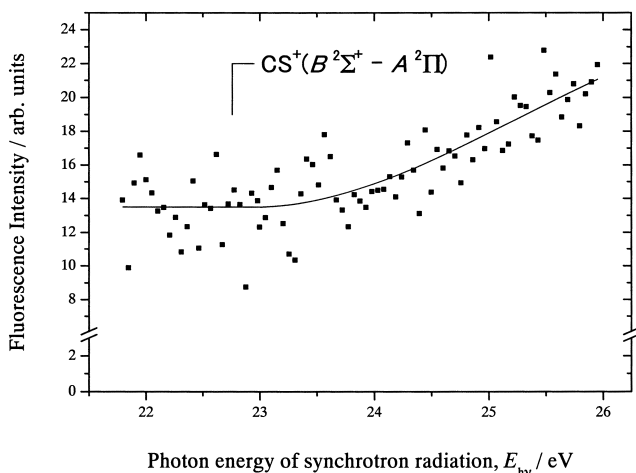


Fig. 4. Fluorescence excitation spectrum of OCS obtained by plotting the fluorescence intensity integrated over the wavelength region of 400–410 nm as a function of E_{hv} . The thermochemical threshold for the formation of $\text{CS}^+(\text{B}^2\Sigma^+) + \text{O}(\text{P}^2)$ from OCS is indicated.

tion of N_2 for the formation of $\text{N}_2^+(\text{B}^2\Sigma_u^+, v' = 0)^{8,31}$ and the branching ratio of 0.7 for the $v' = 0 \rightarrow v'' = 0$ transition.³² A supplementary measurement at $E_{\text{hv}} = 41.7$ eV was made for the normalized count rate, S/ni_{eff} , of the $\text{OCS}^+[\text{A}^2\Pi_{3/2}(0,0,0) \rightarrow \text{X}^2\Pi_{3/2}(0,0,3)]$ emission in order to check the effect of the second-order contamination of the light upon S/ni_{eff} at 20.85 eV. Here, grating G2 (1200 grooves mm^{-1}) was utilized for tuning

the first-order light to $E_{\text{hv}} = 41.7$ eV. We found that S/ni_{eff} at $E_{\text{hv}} = 41.7$ eV is one order of magnitude lower than that at 20.85 eV. This manifests that S/ni_{eff} due to the second-order light is negligibly low at $E_{\text{hv}} = 20.85$ eV.

The cross sections for $\text{OCS}^+[\text{A}^2\Pi_{3/2}(0,0,0) \rightarrow \text{X}^2\Pi_{3/2}(0,0,3)]$, obtained in a similar manner, were found to be $(5\text{--}9) \times 10^{-3}$ Mb at the other photon energies given in Fig. 3. Lee and Judge reported the corresponding cross sections of $(1.0 \pm 0.1) \times 10^{-2}$ Mb at six photon energies between 15.69–19.46 eV.¹³ It is therefore fair to say that the partial photoionization cross section of OCS for the formation of $\text{OCS}^+[\text{A}^2\Pi_{\Omega}(0,0,0)]$ depends rather weakly on the photon energy in the range of from the associated ionization threshold of 15.075 eV to the highest excitation energy in the present measurements, i.e. 29.8 eV.

The above statement is of course true only for the case of direct ionization. The cross section may drastically change across the resonance positions that match the excitation energies for autoionizing superexcited states. This situation can be recognized for the Rydberg series converging to $\text{OCS}^+[\text{B}^2\Sigma^+(0,0,0)]$. Figure 6 shows a fluorescence excitation spectrum for $\text{OCS}^+[\text{A}^2\Pi_{\Omega}(0,0,0) \rightarrow \text{X}^2\Pi_{\Omega}(0,0,3)]$ taken in the E_{hv} range of 15.1–15.75 eV. In this measurement, the 100 mm focal-length monochromator was employed and the signal counts due to the unresolved spin-orbit components, $\Omega = 3/2$ and $1/2$, were added together. The spectrum contains many peaks whose assignments are indicated in Fig. 6, by reference to those given by Leclerc et al.^{33,34} From the same procedure as that described in the preceding paragraphs, we evaluated the

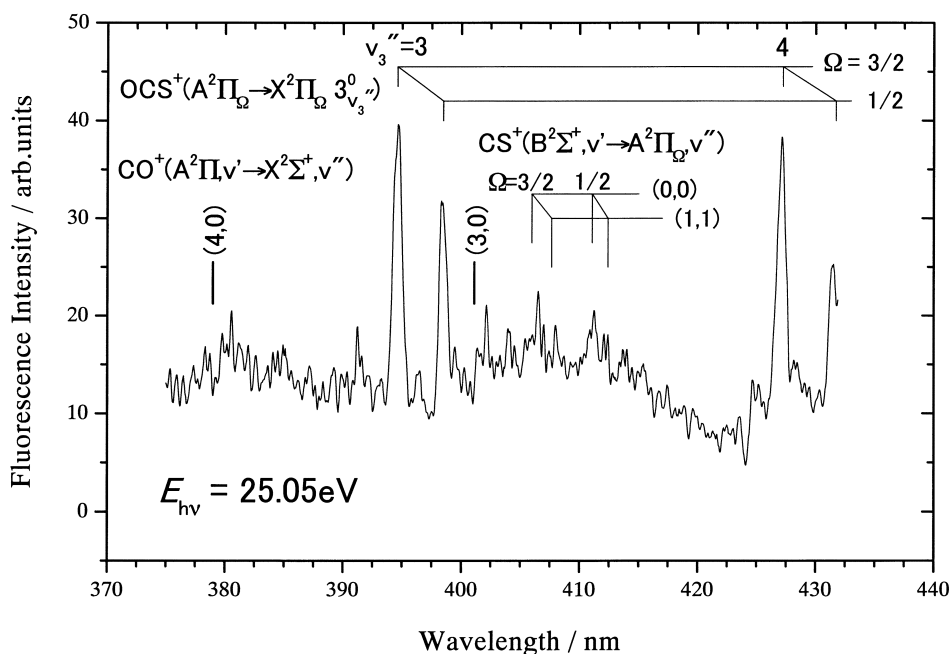


Fig. 5. Dispersed fluorescence spectra of OCS encompassing the wavelength region 375–431 nm at $E_{\text{hv}} = 25.05$ eV. The spectrum was measured by using the imaging spectrograph equipped with a 1200 grooves mm^{-1} grating which has a nominal blaze wavelength of 300 nm. The entrance-slit width was set to 250 μm . The thin short vertical lines indicate two spin-orbit components ($\Omega = 3/2$ and $1/2$) of the vibrational bands of the $\text{OCS}^+[\text{A}^2\Pi_{\Omega}(0,0,0) \rightarrow \text{X}^2\Pi_{\Omega}(0,0,v_3'')]$ transition with $v_3'' = 3$ and 4. The thin long vertical lines indicate the two spin-orbit components of the vibrational bands of the $\text{CS}^+(\text{B}^2\Sigma^+, v' \rightarrow \text{A}^2\Pi_{\Omega}, v'')$ transition (Ref. 24). The (v', v'') mark denotes the band due to the transition from the upper v' to lower v'' vibrational states. The thick vertical lines indicate the band origins of the $\text{CO}^+(\text{A}^2\Pi_{\Omega}, v' \rightarrow \text{X}^2\Sigma^+, v'' = 0)$ emission-band system.

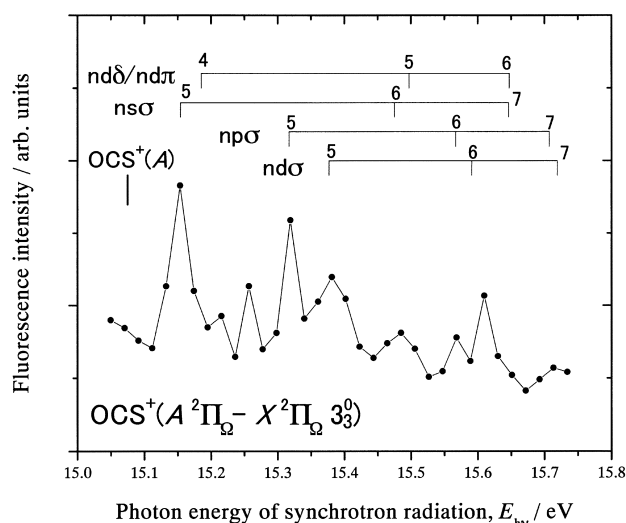


Fig. 6. Fluorescence excitation spectrum of OCS obtained by plotting the fluorescence intensity integrated over the wavelength region of 390–400 nm as a function of E_{hv} . The two spin-orbit components of the $\text{OCS}^+[\text{A}^2\Pi_{\Omega}(0,0,0) \rightarrow \text{X}^2\Pi_{\Omega}(0,0,v_3'' = 3)]$ band are considered to mainly contribute to the observed fluorescence. The thick vertical line indicates the thermochemical threshold for the formation of the vibrational ground state of $\text{OCS}^+(\text{A}^2\Pi_{3/2})$.

fluorescence cross section for $\text{A}^2\Pi_{3/2}(0,0,0) \rightarrow \text{X}^2\Pi_{3/2}(0,0,3)$ to be 0.04 Mb at the $5s\sigma$ Rydberg state ($E_{\text{hv}} = 15.17$ eV). This value is larger by a factor of 4–8 than the cross section for the same transition resulting from the direct ionization of OCS.

Observed Emission at Fluorescence Wavelengths of 530–680 nm. Figure 7 shows the emission spectra obtained from the photoexcitation at four E_{hv} energies from 20.85 to 29.8 eV. In the region 530–680 nm, nine spectral features are discerned: five of them are relatively broad and assignable to rovibrational bands, while the other four have narrow line shape. The bands appearing in the wavelength regions 545–560 nm and 618–635 nm can be assigned to the $v' = 0 \rightarrow v'' = 1$ and $v' = 0 \rightarrow v'' = 2$ transitions of $\text{CO}^+(\text{A}^2\Pi \rightarrow \text{X}^2\Sigma^+)$, respectively, by reference to the reported vibrational energy levels of the ions³⁵ and the Einstein A coefficients for the individual vibrational bands.²² The rest of the broad peaks are attributable to the $\text{CO}(d^3\Delta, v' = 4-6 \rightarrow a^3\Pi, v'' = 0)$ emission-band system.^{35,36} The $\text{CO}^+(\text{A}^2\Pi \rightarrow \text{X}^2\Sigma^+)$ transitions are present at every photon energy larger than 20 eV chosen in the present study, whereas the $\text{CO}(d^3\Delta \rightarrow a^3\Pi)$ transitions are very weak at $E_{\text{hv}} = 22.9$ eV and indiscernible at $E_{\text{hv}} = 20.85$ eV.

The peaks at 582, 596 and 618 nm are narrow and symmetric, which suggests that they arise from atomic transitions. Using the Grotrian diagrams compiled by Bashkin and Stoner,³⁷ we assigned these peaks to the fluorescing transitions from the three consecutive Rydberg states, $\text{S}[nd^3\text{D}^0 \rightarrow 4p^3\text{P}^e]$ ($n = 7-9$). Here, $\text{S}(nd^3\text{D}^0)$ is the member of the Rydberg series converging to the ground $\text{S}^+(\text{S}^0)$ and n denotes the principal quantum number. A similar peak is also seen at 654 nm, and assignable to the transition of the adjacent member of the Rydberg series, $\text{S}(6d^3\text{D}^0 \rightarrow 4p^3\text{P}^e)$. We can then derive a straightforward conclusion that the $\text{S}(nd^3\text{D}^0)$ Rydberg state is pro-

duced not by the dissociation of OCS^+ but by the neutral dissociation of a superexcited state OCS^* of Rydberg type. This is because the primary excitation energy is lower than the dissociation limits of OCS for the formation of $\text{S}[nd^3\text{D}^0]$ ($n = 6-9$) + $\text{CO}^+(\text{X}^2\Sigma^+)$, 27.11–27.34 eV.^{19-21,37}

At $E_{\text{hv}} = 20.85 \pm 0.04$ eV, the peaks located at 582, 596 and 618 nm are no longer observed on the dispersed fluorescence spectrum, whereas there still remains the peak at 654 nm. Hence, the upper limit of the excess internal energy of the counterpart CO fragment is estimated to be 7.75 ± 0.06 eV by using the excitation energy of 9.94 eV for the $\text{S}(6d^3\text{D}^0)$ state³⁷ and the dissociation energy of 3.16 ± 0.015 eV for the formation of $\text{S}^+(\text{P}^e) + \text{CO}(\text{X}^1\Sigma^+)$ from OCS.^{19,20} As listed in Table 1, there are four states of the CO fragment³⁸ whose transition energy (T_{00}) for the 0–0 band with respect to $\text{CO}(\text{X}^1\Sigma^+, v'' = 0)$ is smaller than this upper limit, viz. $\text{X}^1\Sigma^+$, $a^3\Pi$, $a'^3\Sigma^+$, and $d^3\Delta$.

The $\text{CO}(\text{X}^1\Sigma^+)$ ground state is hardly suited for the counterpart of $\text{S}(6d^3\text{D}^0)$ for the following reasons. Photoionization studies of $\text{OCS}(\text{X}^1\Sigma^+)$ have indicated that the potential energy surface of the $\text{OCS}^+(\text{A}^2\Sigma^-)$ state correlating to the lowest dissociation limit of $\text{S}^+(\text{S}^0) + \text{CO}(\text{X}^1\Sigma)$ intersects the potential of $\text{OCS}^+(\text{A}^2\Pi_{\Omega})$ at an ionization energy of ca. 15.1 eV, since any excited vibrational levels of $\text{OCS}^+(\text{A}^2\Pi_{\Omega})$ between 15.18–15.36 eV are known to undergo conversion into the $\text{A}^2\Sigma^-$ state via avoided surface crossings through vibronic coupling to be completely predissociated into $\text{S}^+(\text{S}^0) + \text{CO}(\text{X}^1\Sigma^+)$.^{13,39,40} The Σ^- , Π , and Δ components correlating to the $\text{S}(6d^3\text{D}^0) + \text{CO}(\text{X}^1\Sigma^+)$ limit may behave similarly to the $\text{OCS}^+(\text{A}^2\Sigma^-)$ state along the OC–S dissociation coordinate, if the Rydberg electron of these neutral states has little effect on the bonding of the $\text{A}^2\Sigma^-$ ion core. It is unlikely from these potential relations that the $\text{S}(6d^3\text{D}^0) + \text{CO}(\text{X}^1\Sigma^+)$ channel is accessible by the direct dissociation of the primary OCS^* that was substantiated at $E_{\text{hv}} \geq 20.85$ eV in the present study. Furthermore, there is little probability of the conversion of OCS^* to the Σ^- , Π , and Δ components correlating to $\text{S}(6d^3\text{D}^0) + \text{CO}(\text{X}^1\Sigma^+)$, since the branching ratio of the $\text{S}^+(\text{S}^0) + \text{CO}(\text{X}^1\Sigma^+)$ to $\text{S}^+(\text{D}^0) + \text{CO}(\text{X}^1\Sigma^+)$ channels rapidly decreases with increasing photon energy above the dissociation limit of 15.36 eV for the latter channel.⁴⁰

It is, however, difficult to decide which to select as the most proper counterpart of $\text{S}(nd^3\text{D}^0)$ among the other three states. In the case of $\text{CO}(d^3\Delta)$, the dissociation limit for $\text{S}(6d^3\text{D}^0) + \text{CO}(d^3\Delta)$ is 20.62 ± 0.015 eV, as shown in Table 1. Hence, most of the excess energy at $E_{\text{hv}} = 20.85 \pm 0.04$ eV has been converted preferentially to the electronic energy of CO. This indicates that the involved potential energy curve(s) of OCS should satisfy the following condition: the height of the asymptote $\text{S}(6d^3\text{D}^0) + \text{CO}(d^3\Delta)$ of the dissociation state $\text{OCS}(\text{Dis})$ is included within the Franck–Condon region of the superexcited state OCS^* to which primary photoabsorption takes place. The peaks of $\text{S}(nd^3\text{D}^0)$ with $n \geq 7$ are not observed in the emission spectrum at $E_{\text{hv}} = 20.85 \pm 0.04$ eV. This suggests that the dissociation limit for $\text{S}(7d^3\text{D}^0) + \text{CO}(d^3\Delta)$ of 20.73 ± 0.015 eV is too high to be reached from OCS^* , probably because the nuclear kinetic energy of few hundreds of meV is released in dissociation.

We next examine the possibility of the $\text{S}(6d^3\text{D}^0) + \text{CO}(a'^3\Sigma^+)$ and $a^3\Pi$ channels. The corresponding dissociation

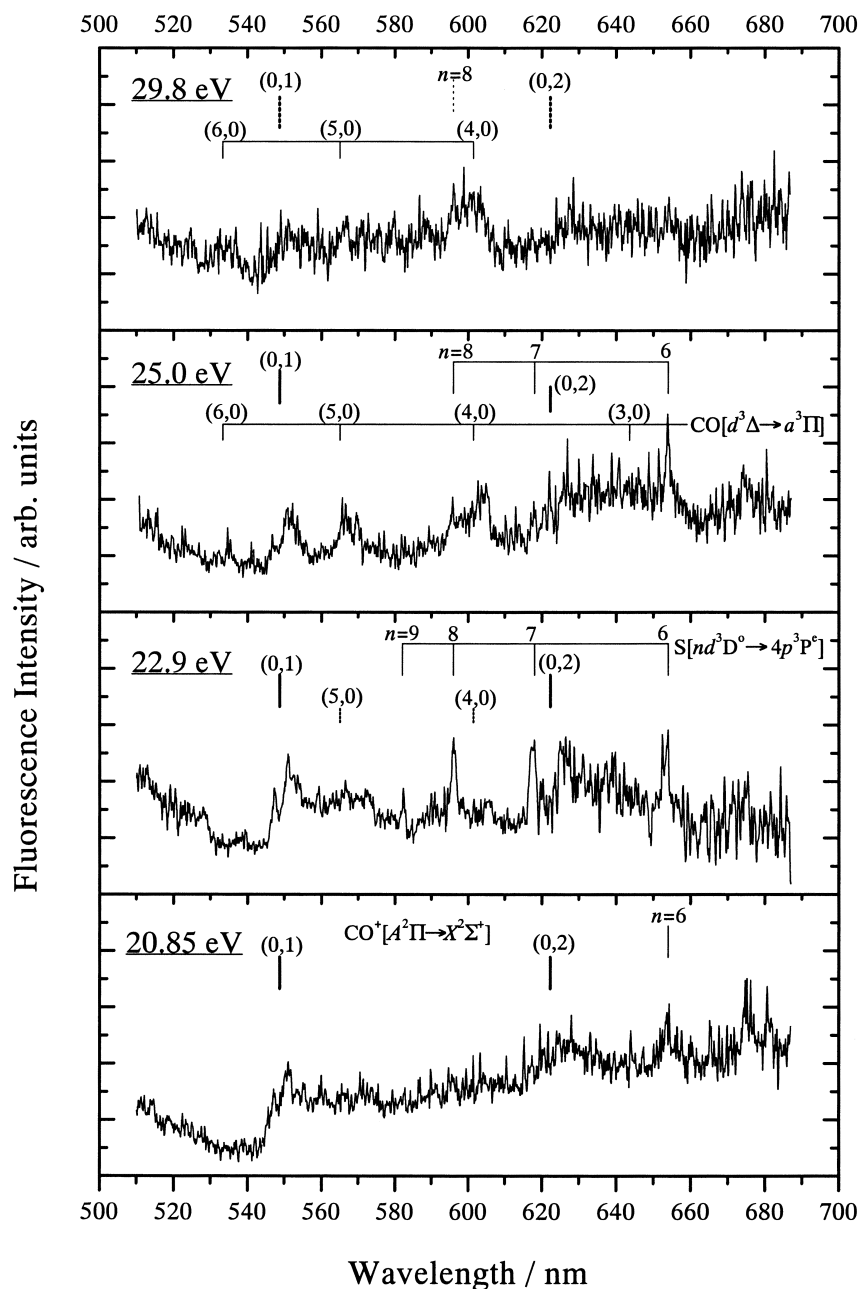


Fig. 7. Dispersed fluorescence spectra of OCS encompassing the wavelength region 530–680 nm at four photon energies between 20.85 and 29.8 eV. The imaging spectrograph equipped with a 600 grooves mm^{-1} grating (blaze wavelength = 500 nm) was used at the entrance-slit width of 250 μm . The thick vertical lines indicate the band origins of the $\text{CO}^+ (A^2\Pi_0, v' = 0 \rightarrow X^2\Sigma^+, v'')$ emission-band system. The $(0, v'')$ mark denotes the band due to the v'' vibrational state of $\text{CO}^+ (X^2\Sigma^+)$. The thin short vertical lines indicate the band origins of the $\text{CO} (d^3\Delta, v' = 3-6 \rightarrow a^3\Pi, v'' = 0)$ band system. The $(v', 0)$ mark denotes the band due to the v' vibrational state of $\text{CO} (d^3\Delta)$. The thin long vertical lines indicate atomic transitions $S [nd^3D^0 \rightarrow 4p^3P^e]$ ($n = 6-9$) where $S (nd^3D^0)$ is the member of the Rydberg series converging to the ground $S^+ (^4S^0)$. The features marked with the dotted lines are less unambiguous.

limits are located at 19.96 ± 0.015 and 19.11 ± 0.015 eV, respectively, and therefore 0.89 ± 0.06 and 1.74 ± 0.06 eV, respectively, are transferred to the vibrational energy of CO and/or kinetic energy with which the fragments fly apart. The intensity distribution of $S (nd^3D^0)$ is determined crucially by the n -dependence of the nonadiabatic transition probabilities at the

avoided surface crossing points formed by the intersection of the potential energy curves of OCS^* and $\text{OCS}(\text{Dis})$. If the Rydberg electron of OCS^* interacts with the ion core and participates directly into the electron-exchange mechanism that controls the conversion at avoided surface crossing points (*participant predissociation*),⁴¹ the energy width for the prediss-

Table 1. Transition Energies T_{00} from the Vibrational Ground State of $\text{CO}(X^1\Sigma^+)$ to That of Low-Lying Electronically Excited States

Electronic state of CO	$T_{00}(\text{CO})^{\text{a}}$	$T_{00}(\text{CO})^{\text{b}}$	$D[\text{S}(6d^3D^0) + \text{CO}]^{\text{c}}$
$X^1\Sigma^+$	0	0	13.10
$a^3\Pi$	6.010	6.010	19.11
$a'^3\Sigma^+$	6.863	6.863	19.96
$d^3\Delta$	7.516	7.519	20.62
$e^3\Sigma^-$	7.898	7.761	21.00
$A^1\Pi$	8.028	8.027	21.13

The fourth column gives the dissociation limits D of $\text{OCS}(X^1\Sigma^+)$ for the formation of $\text{S}(6d^3D^0)$ and the excited states of CO. All energies are in eV.

a) Taken from Ref. 38. b) Taken from the data reported in Ref. 35 on potential energy curves for the electronic states of CO. c) Obtained from the sum of the dissociation energy of 3.16 ± 0.015 eV (Refs. 19 and 20) of $\text{OCS}(X^1\Sigma^+)$ for the formation of $\text{S}(^3P^e) + \text{CO}(X^1\Sigma^+)$, the excitation energy of 9.94 eV (Ref. 37) for $\text{S}(6d^3D^0)$, and $T_{00}(\text{CO})$ in the second column (Ref. 38).

Table 2. Identified Emission-Band Systems in the Vacuum UV Photoexcitation of $\text{OCS}(X^1\Sigma^+)$.

Emitting species	Electronic transition	Vibrational level of the upper state, v'
OCS^+	$A^2\Pi_{\Omega} \rightarrow X^2\Pi_{\Omega}$	0
CO^+	$A^2\Pi_{\Omega} \rightarrow X^2\Sigma^+$	0–4
CS^+	$B^2\Sigma^+ \rightarrow A^2\Pi_{\Omega}$	0, 1
CO	$d^3\Delta \rightarrow a^3\Pi$	4–6
S	$nd^3D^0 \rightarrow 4p^3P^e$	$n = 6\text{--}9^{\text{a}}$

a) Principal quantum number of the Rydberg states of $\text{S}(nd^3D^0)$ observed in Fig. 7.

sociation is expected to be proportional to n^{-3} , since the orbital of the Rydberg electron becomes wider with increasing n . This n -dependence may explain the observation that the branching ratio for predissociation into $\text{S}(nd^3D^0) + \text{CO}(a^3\Sigma^+)$ and $a^3\Pi$ is much smaller at $n \geq 7$ than at $n = 6$. As a future prospect, it is necessary to measure the yield curve of $\text{S}(nd^3D^0)$ for each n as a function of E_{iv} in order to decide on the state of the counterpart CO and to discuss the conversion mechanism of OCS^* to $\text{OCS}(\text{Dis})$.

Summary

By dispersed fluorescence spectroscopy we have studied the fragmentation of OCS into many sorts of emitting species, which follows the vacuum UV photoexcitation at 15–30 eV. Table 2 summarizes the emission-band systems identified in the fluorescence spectra of Figs. 3 and 7. To our knowledge, none of the transitions, except for $\text{OCS}^+(A^2\Pi_{\Omega} \rightarrow X^2\Pi_{\Omega})$, have been reported before in the photoexcitation of OCS above 15 eV. We could offer evidence supporting the neutral dissociation of the Rydberg states of OCS into $\text{S}(nd^3D^0) + \text{CO}(a^3\Pi)$, $a^3\Sigma^+$, and/or $d^3\Delta$ with $n = 6\text{--}9$.

The authors are grateful to Professor Kazutoshi Fukui, Mr. Takayoshi Kihara and the members of the UVSOR facility for helpful advice and discussions during the course of the experiments. This work has been supported financially in part by national funds appropriated for special research projects of the Institute for Molecular Science, by a Grant-in-Aid for Scientific Research (Grant No. 10640504) from the Ministry of Edu-

cation, Science, Sports, and Culture, and by a grant for scientific research from Matsuo Foundation.

References

- I. Nenner and J. A. Beswick, in "Handbook on Synchrotron Radiation," ed by G. V. Marr, North Holland, Amsterdam (1987), Vol. 2, Chap. 6.
- Synchrotron Radiation and Dynamic Phenomena, AIP Conference Proceedings No. 258, ed by J. A. Beswick, Am. Inst. of Phys., New York (1992), Chap. 1.
- J. Berkowitz, E. Rühl, and H. Baumgärtel, in "VUV and Soft X-ray Photoionization," ed by U. Becker and D. A. Shirley, Plenum Press, New York (1996), Chap. 7.
- I. Nenner and P. Morin, in "VUV and Soft X-ray Photoionization," ed by U. Becker and D. A. Shirley, Plenum Press, New York (1996), Chap. 9.
- K. Mitsuke, in "The Physics of Electronic and Atomic Collisions, AIP Conference Proceedings No. 500," ed by Y. Itikawa et al., Am. Inst. of Phys., New York (2000) p. 172.
- D. L. Judge and L. C. Lee, *J. Chem. Phys.*, **57**, 455 (1972).
- D. L. Judge and L. C. Lee, *J. Chem. Phys.*, **58**, 104 (1973).
- A. Tabché-Fouhaile, K. Ito, I. Nenner, H. Fröhlich, and P.-M. Guyon, *J. Chem. Phys.*, **77**, 182 (1982).
- M. Ukai, K. Kameta, S. Machida, N. Kouchi, Y. Hatano and K. Tanaka, *J. Chem. Phys.*, **101**, 5473 (1994).
- M. Ukai, in "Atomic and Molecular Photoionization," ed by A. Yagishita and T. Sasaki, Universal Academy Press, Tokyo (1996), p. 149.
- M. Ukai, S. Machida, K. Kameta, M. Kitajima, N. Kouchi, Y. Hatano, and K. Ito, *Phys. Rev. Lett.*, **74**, 239 (1995).
- Y. Hatano, *Physics Report*, **313**, 109 (1999).
- L. C. Lee and D. L. Judge, *Int. J. Mass Spectrom. Ion Phys.*, **17**, 329 (1975).
- A. Tabché-Fouhaile, M.-J. Hubin-Franskin, J. P. Delwiche, H. Fröhlich, K. Ito, P.-M. Guyon, and I. Nenner, *J. Chem. Phys.*, **79**, 5894 (1983).
- L. C. Lee and D. L. Judge, *J. Chem. Phys.*, **63**, 2782 (1975).
- M. Mizutani, M. Tokeshi, A. Hiraya, and K. Mitsuke, *J. Synchrotron Rad.*, **4**, 6 (1997).
- W. H. Smith, *J. Chem. Phys.*, **51**, 3410 (1969).
- R. G. Bennett and E. W. Dalby, *J. Chem. Phys.*, **32**, 1111

- (1960).
- 19 M. W. Chase, Jr., C. A. Davies, J. R. Downey, Jr., D. J. Frurip, R. A. McDonald, and A. N. Syverud, *J. Phys. Chem. Ref. Data*, **14**, Suppl. No. 1 (1985).
- 20 M.-J. Hubin-Franskin, D. Huard, and P. Marmet, *Int. J. Mass Spectrom. Ion Phys.*, **27**, 263 (1978).
- 21 B. Wannberg, D. Nordfors, K. L. Tan, L. Karlsson, and L. Mattsson, *J. Electron Spectrosc. Relat. Phenom.*, **47**, 147 (1988).
- 22 D. C. Jain, *J. Phys. B*, **5**, 199 (1972).
- 23 D. W. Setser, *Int. J. Mass Spectrom. Ion Phys.*, **11**, 301 (1973).
- 24 M. Tsuji, H. Obase, M. Matsuo, M. Endoh, and Y. Nishimura, *Chem. Phys.*, **50**, 195 (1980).
- 25 M. Tsuji, M. Matsuo, and Y. Nishimura, *Int. J. Mass Spectrom. Ion Phys.*, **34**, 273 (1980).
- 26 H. Sekiya, M. Tsuji, and Y. Nishimura, *Chem. Phys. Lett.*, **100**, 494 (1983).
- 27 H. Sekiya, M. Tsuji, and Y. Nishimura, *Bull. Chem. Soc. Jpn.*, **57**, 3329 (1984).
- 28 I. Tokue, T. Kudo, M. Kobayashi, and K. Yamasaki, *Bull. Chem. Soc. Jpn.*, **70**, 71 (1997).
- 29 N. Jonathan, A. Morris, M. Okuda, K. J. Ross, and D. J. Smith, *Faraday Discuss. Chem. Soc.*, **54**, 48 (1972).
- 30 D. C. Frost, S. T. Lee, and C. A. McDowell, *Chem. Phys. Lett.*, **17**, 153 (1972).
- 31 J. W. Gallagher, C. E. Brion, J. A. R. Samosn, and P. W. Langhoff, *J. Phys. Chem. Ref. Data*, **17**, 9 (1988).
- 32 A. W. Johnson and R. G. Fowler, *J. Chem. Phys.*, **53**, 65 (1970).
- 33 B. Leclerc, A. Poulin, D. Roy, M.-J. Hubin-Franskin, and J. Delwiche, *J. Chem. Phys.*, **75**, 5329 (1981).
- 34 Y. Hikosaka, H. Hattori, T. Hikida, and K. Mitsuke, *J. Chem. Phys.*, **107**, 2950 (1997).
- 35 P. H. Krupenie and S. Weissman, *J. Chem. Phys.*, **43**, 1529 (1965).
- 36 G. W. Taylor, *J. Phys. Chem.*, **77**, 124 (1973).
- 37 S. Bashkin and J. O. Stoner, Jr., "Atomic Energy Levels and Grotrian Diagrams," North-Holland, Amsterdam (1975).
- 38 K. P. Huber and G. Herzberg, "Constants of Diatomic Molecules," Van Nostrand Reinhold, New York (1979).
- 39 J. H. D. Eland, *Int. J. Mass Spectrom. Ion Phys.*, **12**, 389 (1973).
- 40 B. Brehm, R. Frey, A. Küstler, and J. H. D. Eland, *Int. J. Mass Spectrom. Ion Phys.*, **13**, 251 (1974).
- 41 Y. Hikosaka, H. Hattori, and K. Mitsuke, *J. Chem. Phys.*, **110**, 335 (1999).
- 42 J. Delwiche, M.-J. Hubin-Franskin, G. Caprace, P. Natalis, and D. Roy, *J. Electron Spectrosc. Relat. Phenom.*, **21**, 205 (1980).
- 43 K. Mitsuke, S. Suzuki, T. Imamura, and I. Koyano, *J. Chem. Phys.*, **93**, 1710 (1990).
- 44 K. Mizukami, H. Obase, M. Tsuji, and Y. Nishimura, *Chem. Phys. Lett.*, **116**, 510 (1985).
-